Check for updates

Advanced Materials

ADVANCED MATERIALS
www.advmat.de

RESEARCH ARTICLE

A Skin-Inspired High-κ Self-Healing Polymer for Low-Voltage Dielectric Elastomer Actuators

Jian-Cheng Lai[1] | Eunyoung Kim[1,2] | Chengyi Xu[1] | Simiao Niu[3] | Yuanwen Jiang[1] | Donglai Zhong[1] | Yucan Peng[4] | Weichen Wang[1] | Zhitao Zhang[1] | Christopher B. Copper[1] | Huaxin Gong[1] | Hongping Yan[1] | Yangju Lin[1] | Deyu Liu[1] | Chuanzhen Zhao[1] | Can Wu[1] | Yuelang Chen[1,5] | Song Zhang[1] | Yu Zheng[1] | Gan Chen[4] | Fuying Dong[3] | Jeffrey B.-H. Tok[1] | Zhenan Bao[1]

[1]Department of Chemical Engineering, Stanford University, Stanford, California, USA | [2]Department of Mechanical Engineering, Stanford University, Stanford, California, USA | [3]Department of Biomedical Engineering, Rutgers University, Piscataway, New Jersey, USA | [4]Department of Materials Science and Engineering, Stanford University, Stanford, California, USA | [5]Department of Chemistry, Stanford University, Stanford, California, USA

Correspondence: Zhenan Bao (zbao@stanford.edu)

Received: 10 December 2025 | **Revised:** 24 June 2026 | **Accepted:** 1 August 2026

Keywords: dielectric elastomer actuators | high dielectric constant elastomers | self-healing

ABSTRACT

Dielectric elastomer actuators (DEAs), known as a type of artificial muscles, are promising soft actuators with many applications including robotics and wearables due to their conformability, fast response, and large actuation. However, their usage remains constrained by high driving voltages needed to achieve substantial actuation. Here, we design a skin-inspired high-κ self-healing elastomer, poly-(acrylonitrile-co-butadiene)-co-thiourea (PABTU), that features a high dielectric constant (15 at 1 kHz), low Young's modulus (0.58 and 0.012 MPa upon pre-stretch), and ability to form pinhole-free thin films (~ 3 μm). To mitigate relatively high dielectric loss of our PABTU, PABTU/PDMS-MPU$_{0.3}$-IU$_{0.7}$ bilayer structure (ULTRA) is used for actuators, increasing its breakdown strength from ~33 to 43 V/μm. Our ULTRA actuators exhibit visible deformation at an unprecedented low voltage of 30 V and an areal strain exceeding 130% at 120 V, representing an order of magnitude reduction in voltage for actuation compared with previously reported DEAs while achieving similar actuation strain. As proof of concept, we demonstrate a low-voltage multipixel array with ULTRA DEA. Our molecular design concept provides a path for material systems toward low-voltage operating soft robotics.

1 | Introduction

Dielectric elastomer actuators (DEAs) also known as artificial muscles, generate mechanical deformation when a high voltage applied across compliant electrodes compresses the dielectric elastomer through Coulombic attraction force and drives lateral expansion due to the elastomer's incompressibility (Figure 1a). Compared to rigid actuators, DEAs offer advantages, including conformal contact with curved human body surfaces, compactness, a wide operating frequency range, fast response speed, and high actuation strain [1–3]. However, current DEA materials can only achieve high actuation strains (e.g. ~ 100 %) under high driving voltages (in kVs), tens to hundreds of times higher than the human safe voltage [4–8]. Therefore, achieving low-voltage operation remains a critical yet unaddressed challenge. The actuated strain (S_a) of DEAs in the out-of-plane direction can

Jian-Cheng Lai, Eunyoung Kim, Chengyi Xu, and Simiao Niu contributed equally to this work

All rights reserved, including rights for text and data mining and training of artificial intelligence technologies or similar technologies.
© 2026 Wiley-VCH GmbH

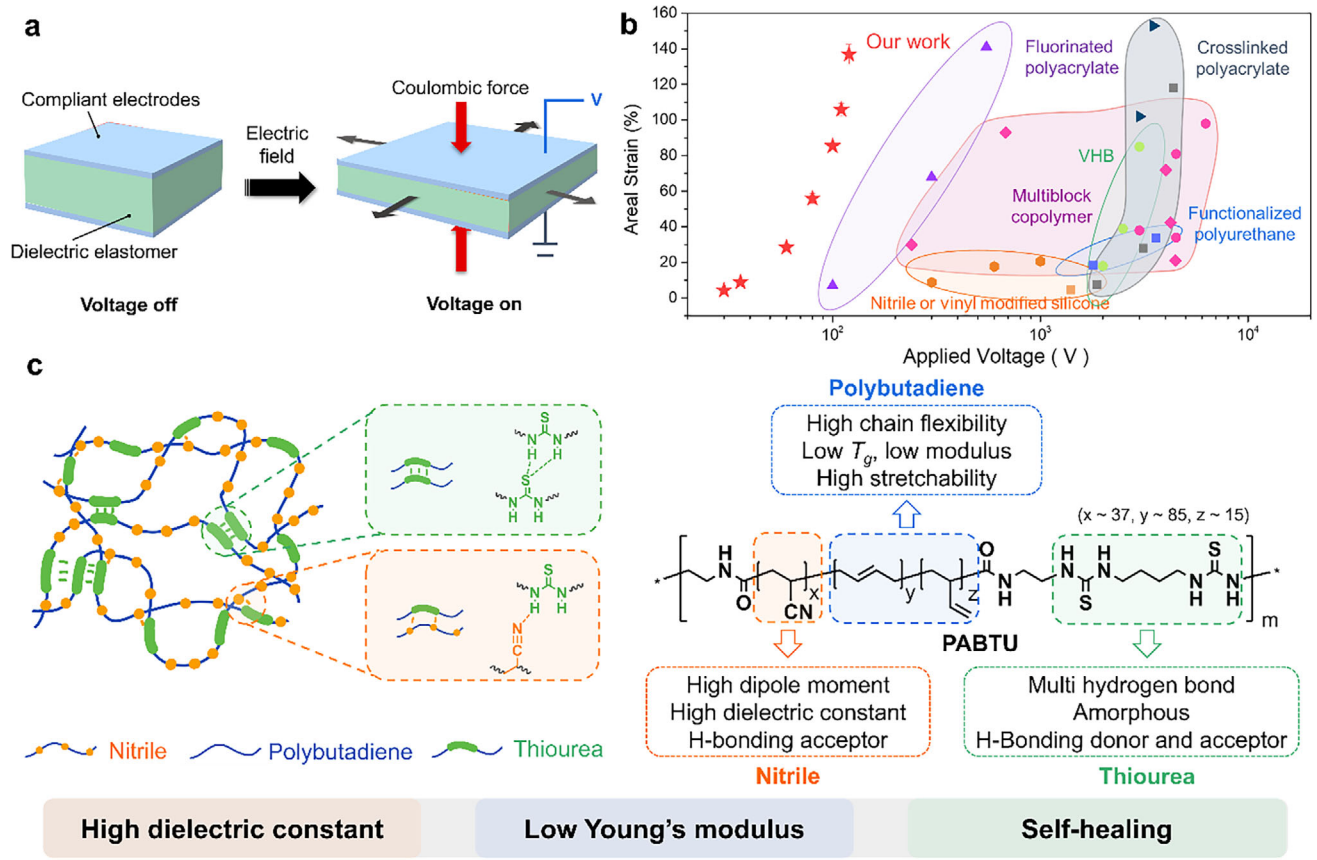

FIGURE 1 | Design of high-κ self-healing poly-(acrylonitrile-co-butadiene)-co-thiourea (PABTU) polymer. (a) Illustration of the DEA working mechanism. (b) Comparison of actuated area strain as a function of applied voltage among functionalized polyurethane [15], nitrile or vinyl modified silicone [16, 17], crosslinked polyacrylate [18, 19], fluorinated polyacrylate [22], and multiblock copolymer [20, 21]. (c) Polymer design and features of the synthesized PABTU polymer.

be estimated by Equation (1):

$$S_a = \frac{\varepsilon_0 \kappa}{E}\left(\frac{V}{t}\right)^2 \quad (1)$$

where ε_0 is the vacuum permittivity, κ is the relative permittivity (dielectric constant) of the dielectric elastomer, V is the voltage applied across the dielectric elastomer film, t is the film thickness and E is Young's modulus of the dielectric elastomer [9–12]. Based on Equation (1), to effectively reduce the driving voltage with large actuation, it is desirable for the dielectric elastomers to have high dielectric constants (κ), low Young's moduli, and minimized thicknesses [1, 13, 14]. However, previously reported dielectric elastomers achieved improvements only on one or two of the above three features. They are still not able to realize both low voltage actuation and large areal actuation at the same time.

Commonly used DEA materials, such as VHB ($\kappa \sim 4.7$ at 1 Hz), and PDMS ($\kappa \sim 3.2$ at 1 Hz), can only partially meet the above stringent requirements, motivating the development of better dielectric elastomers. Previously, a PDMS-based ultrathin DEA reduced the driving voltage from 3.3 kV to 245 V with 7.5% lateral strain by decreasing the thickness from 30 to 3 μm [14], but its dielectric constant and Young's modulus were not improved, preventing further voltage reduction needed for large actuation. We previously showed that introducing self-healing properties through dynamic noncovalent crosslinking of the polymer network self-healed pinhole generated due to electrical breakdown, and recovered DEA function [7]. This suggests self-healing property is desirable in DEA elastomers. A functionalized polyurethane with hierarchical hydrogen bonds demonstrated superior mechanical robustness and self-healing properties, achieving a dielectric constant of ~9 and a Young's modulus of 1.49 MPa. However, its actuation was still limited to ~34% at kV ranges [15]. In other approaches, the mechanical properties of vinyl-modified polysiloxanes were designed for solvent-free thin-film fabrication (~ 100s μm thick), while nitrile-modified polysiloxanes were incorporated with polar nitrile groups to attain a high dielectric constant of ~18, resulting in an actuation of ~20% at 1 kV [16, 17]. Several crosslinked polyacrylates with dielectric constants ~6 with Young's moduli ranging from tens kPa to a few MPa were prepared through various strategies such as using macromolecular crosslinkers and bimodal networks [18, 19]. Among them the polyacrylate with a bimodal network structure showed a large actuation strain of ~160%, although they had to be operated at 3.5 kV [19]. Moreover, multiblock copolymers were developed to tune both mechanical and dielectric properties, exhibiting 30% area strain at 240 V [20, 21]. Recently, a high-performance fluorinated polyacrylate with a dielectric constant of 10.23 enabled actuation at 100 V [22]. However, small actuation of ~ 7% was obtained at low voltage (100 V), highlighting the ongoing challenge of achieving

15214095, 0, Downloaded from https://advanced.onlinelibrary.wiley.com/doi/10.1002/adma.202523659 by Peking University Health, Wiley Online Library on [30/08/2026]. See the Terms and Conditions (https://onlinelibrary.wiley.com/terms-and-conditions) on Wiley Online Library for rules of use; OA articles are governed by the applicable Creative Commons License

large actuation at reduced operating voltage (Figure 1b). Here, we report a high-κ self-healing poly-(acrylonitrile-co-butadiene)-co-thiourea (PABTU) polymer (Figure 1c) with a high dielectric constant ($\kappa \sim 15$ at 1 kHz). Its autonomous self-healing property helps to reduce thin film defects/pinholes, enabling the fabrication of ultrathin DEAs. Furthermore, the polymer has a low Young's modulus (0.58 ± 0.02 MPa), high stretchability (elongation of 2900 %), high breakdown strength (187.3 ± 5.3 MV m^{-1}), and high fracture energy (32.95 kJ m^{-2}). This material enabled low voltage actuation at 120 V (0.5 Hz), generating large area strain of 136.9 % (Figure 1b). This voltage range is an order of magnitude lower compared to previously reported DEAs with similar actuation strains. Moreover, area strains of 28.5% and 4.3% can be achieved at as low as 60 and 30 V, respectively. As a proof of concept, a multipixel DEA array was demonstrated using the low voltage dielectric elastomer actuators.

2 | Results and Discussion

2.1 | Material Design

To achieve a high-κ self-healing elastomer, we designed a poly-(acrylonitrile-co-butadiene)-co-thiourea (PABTU) (M_n = 31500, M_w = 54500) (Figure 1c). Briefly, an amine-terminated poly (acrylonitrile-co-butadiene) (APAB) was prepared from the carboxyl-terminated poly(acrylonitrile-co-butadiene) (CPAB) followed by reacting with the 1,4-butane diisothiocyanates to obtain PABTU (See Experimental Section and Note 1-2, Figures S1–5 for more details). The rationales for PABTU design are: (i) The nitrile segments are chosen for their high dipole moments (4.01 D) to provide high dielectric constant; (ii) the flexible polybutadiene segments are used to give low glass transition temperature (T_g), low Young's modulus and stretchability; (iii) the thiourea segments and amides should provide abundant hydrogen bonds, resulting in self-healing properties (Figure 1c). Furthermore, thiourea groups instead of ureas were chosen as they should produce lower Young's modulus polymer networks because they do not form long-range ordered H-bonding nanostructures [23, 24]. Finally, the periodic placement of the H-bonding thiourea groups provide notch-insensitivity, high stretchability and toughness as we previously reported [7, 25, 26]. The PABTU film (~100 μm thick) is transparent with >97 % transmittance in both visible and near-infrared wavelength range (Figure S6).

2.2 | Mechanical and Self-Healing Properties

PABTU exhibited excellent mechanical properties. First, it exhibits a glass transition temperature (T_g) of ~ −36.5°C (Figure S7). Under a strain between 100% and 500%, the stress relaxation stabilized after 20 min (Figure 2a), maintaining at around 50%–60% of the maximum stress value (Figure S8). The time-temperature superposition (TTS) of rheological curves of G' and G′ at different temperatures give the characteristic relaxation time (τ) (Figure S9). τ at 25°C was found to be as long as 6 × 10^6 s, which indicates that PABTU can maintain residual stress for a long time when kept in a stretched state at room temperature. To show the reversibility of PABTU in the actuation range, Figure S10 shows cyclic stretching tests of PABTU with various stretching ratios and rates after prestretched to 400%. After 400% prestrain, the hysteresis in the first 10 cycles of 100% strain decreased by ~62%, from 2.04 to 0.78 MJ/m^3. The hysteresis was relatively stabilized after 10 s of cycles showing 8% decrease in hysteresis from 0.50 to 0.46 MJ/m^3 at 50th and 100th cycles, respectively. Second, PABTU exhibited high stretchability up to 2900% strain at a loading rate of 2000% min^{-1} at room temperature (Figure 2b). Third, the Young's modulus of PABTU is low, comparable to skin (0.58 ± 0.02 MPa, Figure S11 and Table S1). Moreover, by applying the prestretch ($\lambda = 4$), the Young's modulus significantly decreased to 0.012 MPa, which could contribute to low voltage actuation (Figure S12). Fourth, PABTU showed a high toughness (11.23 MJ m^{-3}), high fracture energy (32.95 kJ m^{-2}), and notch insensitiveness (Figure 2b,d and Figure S13). The above combination of properties makes PABTU an excellent candidate for DEA, suggesting its potential for high tolerance to large deformation, wear and tear that are common for DEA devices.

In addition, PABTU exhibits fast and autonomous self-healing at room temperature. Specifically, after only 1 min, the cut pieces of PABTU already healed and can withstand ~ 500% strain (Figure S15a and Video S1). Healing for 4 h led to a recovered fracture strain of 2750% and a high healing efficiency (η) of 94.6 % (Figure 2c). Damage on the PABTU film started to show the closing of the open regions after just 5 min and the opening completely disappeared after 4 h (Figure 2e,f). Since hydrogen bonds can still re-form at newly cut surfaces, a square sample healed this way can be stretched again to about 400% strain after healing for only 1 min (Figure 2g and Video S2).

Mechanical stability under high humidity or water environment is also a challenge for skin-integrated DEA interface because it inevitably contacts with water, sweat, or moisture vapor on the skin. Remarkably, the underwater healing efficiency of the PABTU was observed to be similar to that in air (Figure 2h). Specifically, PABTU film (~ 500 μm thick) was able to maintain its original mechanical properties (i.e. almost unchanged stress–strain curve) after being immersed in water for 24 h (Figure S14). This may be attributed to the presence of ~ 70 wt% of the hydrophobic polybutadiene segments in the polymer. It can withstand 500 % strain after healing underwater for 1 min (Figure S15b) and almost recovered its original mechanical properties after 4 h (Figure S16 and Video S3). Remarkably, an air or water-filled balloon with a PABTU polymer film as the fast-healing protection layer can withstand puncture by a sharp needle without leaking air or gushing water (Figure 2j,k and Video S4).

Even an ultrathin 1 μm thick freestanding PABTU film could withstand 1500 % strain, and remained undamaged by a needle, unlike other typical elastomers, such as PDMS (Figure 2i, Figure S17 and Video S5). The superior mechanical properties of PABTU are attributed to the multiple types of hydrogen bond units that may be possible within the network, such as thiourea, amides, and —CN [27], which provide multiple modes of energy dissipation under strain. Replacing thiourea with urea or changing poly(acrylonitrile-co-butadiene) to polybutadiene as the backbone both resulted in poorer healing efficiency and lower fracture energy (See more details in Note 3 and Figures S18,19). A recent report also presented a fast-healing elastomer, however, its mechanism was different, based on electrostatic interactions and

15214095, 0, Downloaded from https://advanced.onlinelibrary.wiley.com/doi/10.1002/adma.202523659 by Peking University Health, Wiley Online Library on [30/08/2026]. See the Terms and Conditions (https://onlinelibrary.wiley.com/terms-and-conditions) on Wiley Online Library for rules of use; OA articles are governed by the applicable Creative Commons License

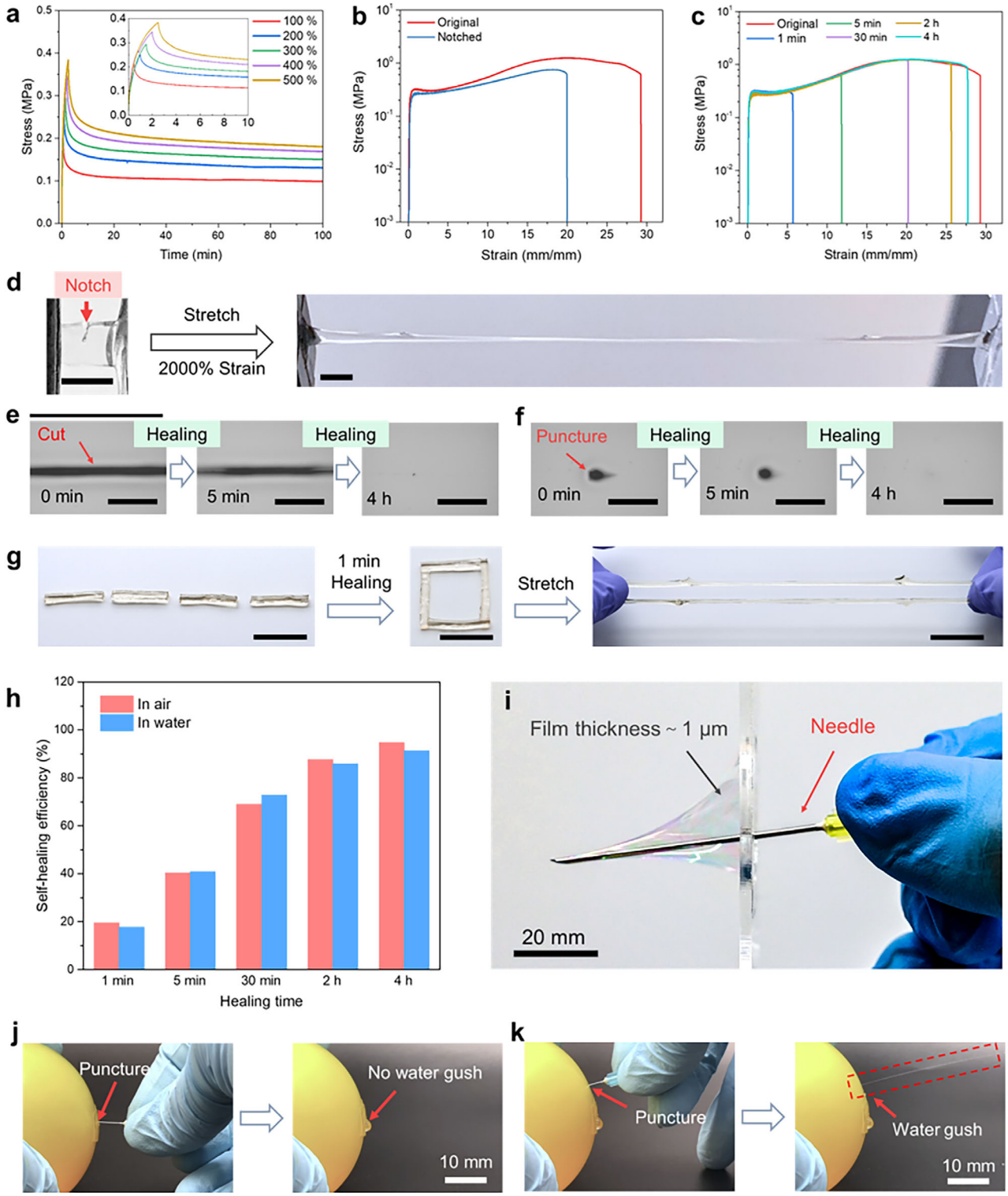

FIGURE 2 | Mechanical and self-healing properties of PABTU. (a) Stress-relaxation curves of PABTU under different strain (Inset: Zoom-in stress-relaxation curves from 0 to 10 min). (b) Stress–strain curves of original and notched PABTU. (c) Strain–stress curves of original and healed PABTU. The PABTU films healed at 25°C for different time intervals. An obvious self-healing behavior at 5 min was observed and healing was completed after 4 h at 25°C. (d) Photographs of notch insensitivity of PABTU (scale bars: 5 mm). (e, f) Optical microscope images of the cut (e) and punctured (f) PABTU films (scale bars: 400 μm). (g) The photographs showing self-healing property between fresh-cut and old surfaces of PABTU (scale bars: 20 mm). (h) Healing efficiencies of PABTU after various healing time under air and water conditions. The healing efficiency η was calculated from the fracture strain ratio of the healed one (S_H) to the original one (S_O), with the equation of $\eta = (S_H/S_O) \times 100\%$. (i) The demonstration of mechanical stability of PABTU film (thickness ~ 1 μm). (j, k) The demonstration of fast self-healing induced sealing property of PABTU. We attached a piece of PABTU polymer film (thickness ~ 200 μm) to a balloon filled with water. When the needle pricked the area covered by PABTU, there was no water gush (j). When the needle pricked the area without PABTU, water gushed out as a continuous flow (k).

15214095, 0, Downloaded from https://advanced.onlinelibrary.wiley.com/doi/10.1002/adma.202523659 by Peking University Health, Wiley Online Library on [30/08/2026]. See the Terms and Conditions (https://onlinelibrary.wiley.com/terms-and-conditions) on Wiley Online Library for rules of use; OA articles are governed by the applicable Creative Commons License

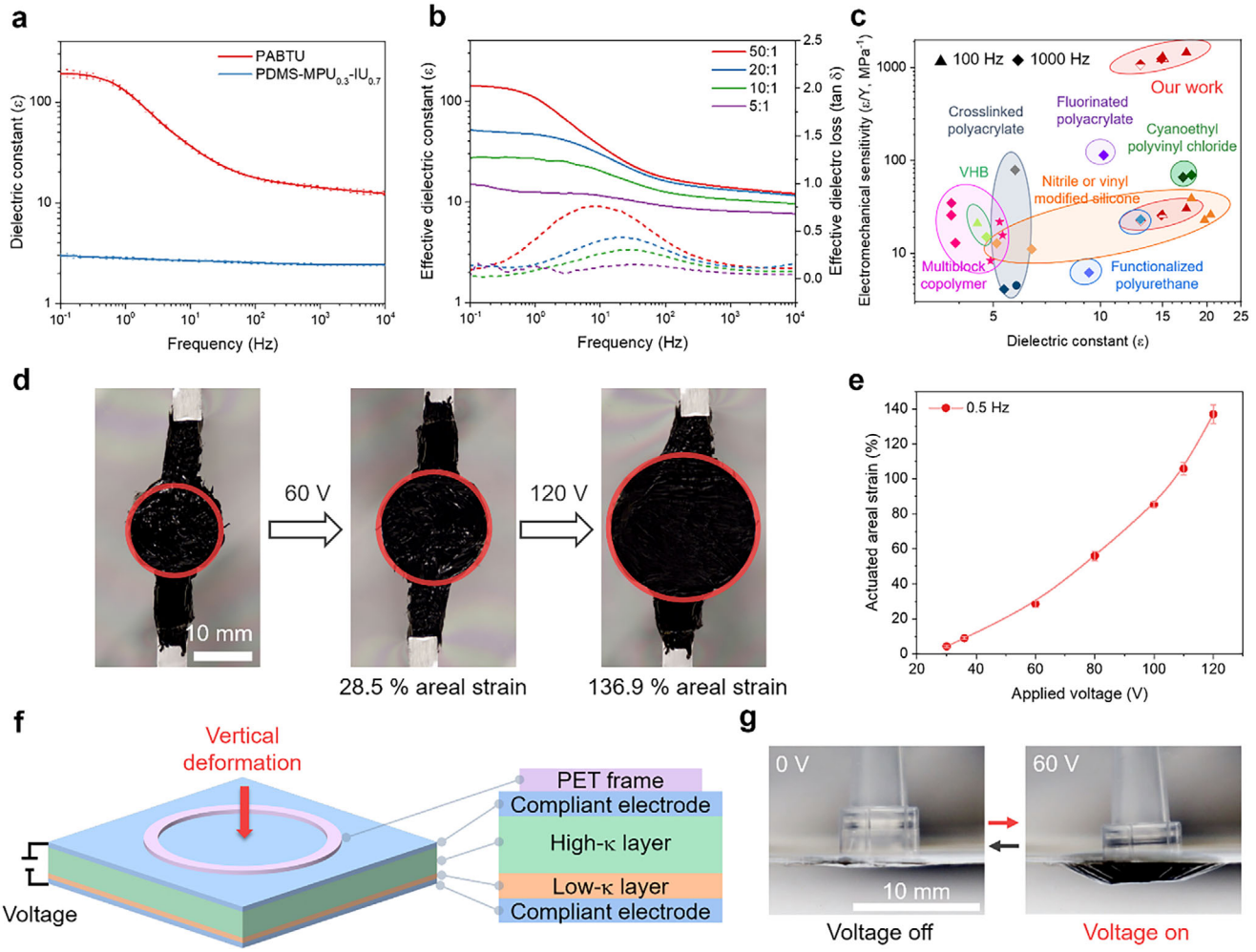

FIGURE 3 | Dielectric property of PABTU and actuation performance of PABTU-based bilayer DEA (ULTRA). **(**a) Dielectric constant of the PABTU and PDMS-$MPU_{0.3}$-$IU_{0.7}$ at various frequencies. (b) Effective dielectric constant and dielectric loss of PABTU/PDMS-$MPU_{0.3}$-$IU_{0.7}$ bilayer. (c) Comparison of the electromechanical sensitivity and dielectric constant among functionalized polyurethane [15], nitrile or vinyl modified silicone [16, 17], crosslinked polyacrylate [18, 19], multiblock copolymer [20, 21], fluorinated polyacrylate [22], and cyanoethyl polyvinyl chloride [37] (Full color: PABTU and half-filled: PABTU/PDMS-$MPU_{0.3}$-$IU_{0.7}$ bilayer (20:1)). (d) Photographs of ULTRA under 60 and 120 V, showing areal strain of 28.5% and 136.9%, respectively. (e) Dependence of actuated areal strain on the applied voltage for the ULTRA at 0.5 Hz. (f) The schematic illustration of ULTRA-V. (g) Photographs of the loading (100 mg) bearing ULTRA under 0 and 60 V at 0.5 Hz.

the softening of polymer chains to enhance segmental motion in the presence of water molecules [28].

2.3 | Dielectric Property of PABTU

PABTU exhibited a high dielectric constant across a wide range of frequencies (Figure 3a). In the low-frequency range, the dielectric constant of PABTU reached 128.9 ± 7.5 at 1 Hz. The steep increase in dielectric constant at low frequency (<100 Hz) may arise from interfacial polarization (Note 5 and Figure S22) [13, 29 30]. Also, in the high-frequency range, the dielectric constant of PABTU (14.9 ± 0.7 at 1 kHz) was ~ 6-time higher compared to PDMS ($\kappa \sim 2.5$ at 1 kHz) and ~ 3-time higher than VHB ($\kappa \sim 4.7$ at 1 kHz), both commonly used commercial dielectric elastomers for DEAs [31, 32]. Although PABTU exhibits high κ, due to the presence of high polarity -CN groups, the dielectric loss of PABTU is expected to be higher than low-κ elastomers, such as PDMS, and may have a larger leakage current and more dielectric loss (Figure S20). This trade-off between high dielectric constant and low dielectric loss makes it challenging to achieve both low driving voltage with large actuation. To address this issue, we prepared DEAs using a PABTU-based bilayer structure by passivating the high κ PABTU with a much thinner low-κ layer (~200 nm) of a self-healing PDMS-$MPU_{0.3}$-$IU_{0.7}$ polymer [33] with excellent stretchability, notch-insensibility property and similar Young's modulus as PABTU H-bonding moieties in both polymers allow easy bonding and good adhesion with each other [33]. The effective dielectric constant and dielectric loss of PABTU/PDMS-$MPU_{0.3}$-$IU_{0.7}$ bilayer with different thickness ratios are shown in Figure 3b and Figure S21. As PABTU to PDMS-$MPU_{0.3}$-$IU_{0.7}$ thickness ratio decreases from 50:1 to 5:1, both effective dielectric constant and dielectric loss decrease. A PABTU to PDMS-$MPU_{0.3}$-$IU_{0.7}$ at a 20:1 thickness ratio was used for PABTU-based bilayer DEAs (ULTRA) fabrication because it provides lower dielectric loss to reduce heating and increased

15214095, 0, Downloaded from https://advanced.onlinelibrary.wiley.com/doi/10.1002/adma.202523659 by Peking University Health, Wiley Online Library on [30/08/2026]. See the Terms and Conditions (https://onlinelibrary.wiley.com/terms-and-conditions) on Wiley Online Library for rules of use; OA articles are governed by the applicable Creative Commons License

dielectric breakdown strength from ~33 to 43 V/μm, while maintaining a high dielectric constant (13.1 at 1 kHz). Combining PABTU's low modulus and high dielectric constant, ULTRA presented high electromechanical sensitivity β (defined as κ/E, a key parameter to evaluate DEA performance [34–36]) (1241.7 and 25.7 at 1 kHz, using Young's moduli with and without prestretch, respectively) (Figure 3c). In addition, the autonomous self-healing property increased the voltage tolerance for the thin films compared to high-κ polymer without self-healing capabilities due to self-healing of potential pinholes. Specifically, a ultrathin film (~500 nm thickness) of PABTU coated on silicon wafer (Figure S23) showed a higher breakdown strength of 187.3 ± 5.3 V/μm compared to a commercially available high-κ elastomer Nitrile rubber (NBR, 109.4 V/μm), and Poly(vinylidene fluoride-co-hexafluoropropene) (P(VDF-HFP), 81.0 V/μm), measured under the same conditions. As another comparison, a low-κ polymer crosslinked PDMS (Sylgard 184) measured by a similar method showed a breakdown strength of 200.3 V/μm. Possessing both high-κ and high breakdown strength are particularly desired due to the high electrical field required.

2.4 | Actuation Performances of ULTRA

The PABTU/PDMS-$MPU_{0.3}$-$IU_{0.7}$ (20:1) bilayer elastomer film (~ 42 μm thickness) was equiaxially prestretched to four times its original diameter to a final film thickness of ~3 μm to make ULTRA actuators. By integrating this prestretched elastomer with two carbon grease compliant electrodes, we fabricated ULTRA (Figure S24). Upon applying a voltage, the dielectric elastomer deformed in the thickness direction and resulted in an expansion in the in-plane direction due to Maxwell stress (Figure S25). A square wave with the amplitude ranging from 30 to 120 V and frequency of 0.5 Hz was applied. The areal strain (S_a) was calculated by the ratio of the area expansion of the electrode (A_e) to the original area of the electrode (A_o), which is $S_a = (A_e\text{-}A_o)/A_o$. The ULTRA realized approximately 4.3%, 28.5%, and 136.9% area strain with applied voltages of 30, 60, and 120 V, respectively (Figure 3d,e, Figure S26 and Video S6). The voltage required to achieve large area strain here is significantly less than previously reported DEAs (Figure 3i), and ULTRA is the first-reported DEA that achieved apparent deformation under 36 V, and over 100% areal strain under 120 V. The bilayer increased the DEA breakdown voltage from ~ 100 to 130 V, corresponding to an increase in breakdown strength from ~ 33 to 43 V/μm, arising from reduced effective dielectric loss with PABTU/PDMS-$MPU_{0.3}$-$IU_{0.7}$ bilayer. It is noted that the breakdown field measured in a DEA is substantially lower than that of the thin film earlier supported on a silicon substrate due to different device geometry. The reduced leakage current in the bilayer compared to a single-layer film is expected to result in less Joule heating, which was confirmed by a much less observed temperature rise (Figure S27). The bilayer structure reduces dielectric loss-induced heating that can cause electrical breakdown. Furthermore, ULTRA showed high actuated area strain over a wide frequency range from 0.1 to 200 Hz (100 V square wave applied voltage) and actuated areal strain decreased as the frequency increased (Figure S28 and Video S7). At 100 V, the areal strain decreased from 103.7% at 0.1 Hz to 57.2 % at 5 Hz, indicating that at higher frequencies the dielectric elastomer does not have sufficient time to fully actuate due to its viscoelastic behavior, resulting in reduced areal strain. This frequency dependent actuation is commonly found in DEAs [38–40].

Compared with the state of the art dielectric elastomers, PABTU exhibited high electromechanical sensitivities, particularly in the prestretched state where the modulus is very low (0.012 MPa), resulting in an order of magnitude higher electromechanical sensitivity (Figure 3c) [7, 14–22, 37]. A previously reported fluorinated polyacrylate showed relatively high electromechanical sensitivity, attributed to its relatively high dielectric constant of ~ 10 with low Young's modulus of ~ 0.09 MPa [22]. However, its actuation strain was limited to <10 % at 100 V, whereas our ULTRA achieved 87.1% at 100 V. This may be enabled by the ability to fabricate thin film with low modulus in the prestretched state and high breakdown field from reduced film pinhole due to the self-healing property. Cyanoethyl poly(vinyl chloride) has also been reported with a high dielectric constant of 18.9 with ~ 0.3 MPa, however, its actuation was limited to ~ 12% area strain with a low breakdown strength of 19.53 V/μm [37], compared to 43 V/μm of our ULTRA.

To achieve deformations only in the vertical direction, we designed an ULTRA actuator for vertical deformation (ULTRA-V) by adding a rigid polyethylene terephthalate (PET) frame to constrain the in-plane expansion of the actuator (Figure 3f). The load bearing property was tested by adding a 0.1 g item and applying a square wave voltage. The ULTRA-V with 0.1 g load generated millimeter-range vertical deformation under low driving voltages of 30 to 72 V at 0.5 Hz (Figure 3g, Figure S29a and Video S8). Specifically, the actuated displacement reached as high as 1.52 mm at 0.1 g load when the driving voltage was 60 V (Figure 3g). Finally, ULTRA-V produced distinct vertical displacement under different frequencies (0.5 to 60 Hz) (Figure S29b and Video S9). As the frequency increased, the vertical displacement decreased, similar to planar actuation behavior.

In addition, polymer composites with high-κ filler materials can further reduce the driving voltage because of the enhanced dielectric constants. However, such composite materials usually suffer from large leakage currents due to inhomogeneous composition. Benefiting from the self-healing property and high fracture energy of PABTU, its polymer composite film with 10 wt% $SrTiO_3$ (PABTU-ST10) showed excellent stretchability and toughness, with the maximum strain 2310 ± 80 % and toughness 7.63 ± 1.06 MJ m^{-3} (Figure S30 and S31). The as-prepared PABTU-ST10 polymer composite film was white in color and became a uniform opaque film during the prestretch process, indicating the nanoparticles dispersed well in the PABTU matrix (Figure S32). The dielectric constant of the as-prepared PABTU-ST10 was effectively increased (Figure S33) but it's Young's modulus (0.50 ± 0.05 MPa) remained about the same level. The drive voltage of the PABTU-ST10-based ULTRA (ULTRA-ST) can be further decreased. The areal strain reached 4.8 % with a voltage as low as 20 V, 10.1 % under 30 V and 39.2 % under 60 V at the frequency of 0.5 Hz (Figure S34), which created new low-voltage records for DEAs. ULTRA-ST showed stable actuation performances over 1000 s of actuation cycles, demonstrating the material reliability and fatigue resistance (Figure S35).

Finally, DEA can serve as a core component for haptic functions by applying various levels of forces on skin via applied voltages and frequencies. The top elastomer layer and bottom actuator

15214095, 0, Downloaded from https://advanced.onlinelibrary.wiley.com/doi/10.1002/adma.202523659 by Peking University Health, Wiley Online Library on [30/08/2026]. See the Terms and Conditions (https://onlinelibrary.wiley.com/terms-and-conditions) on Wiley Online Library for rules of use; OA articles are governed by the applicable Creative Commons License

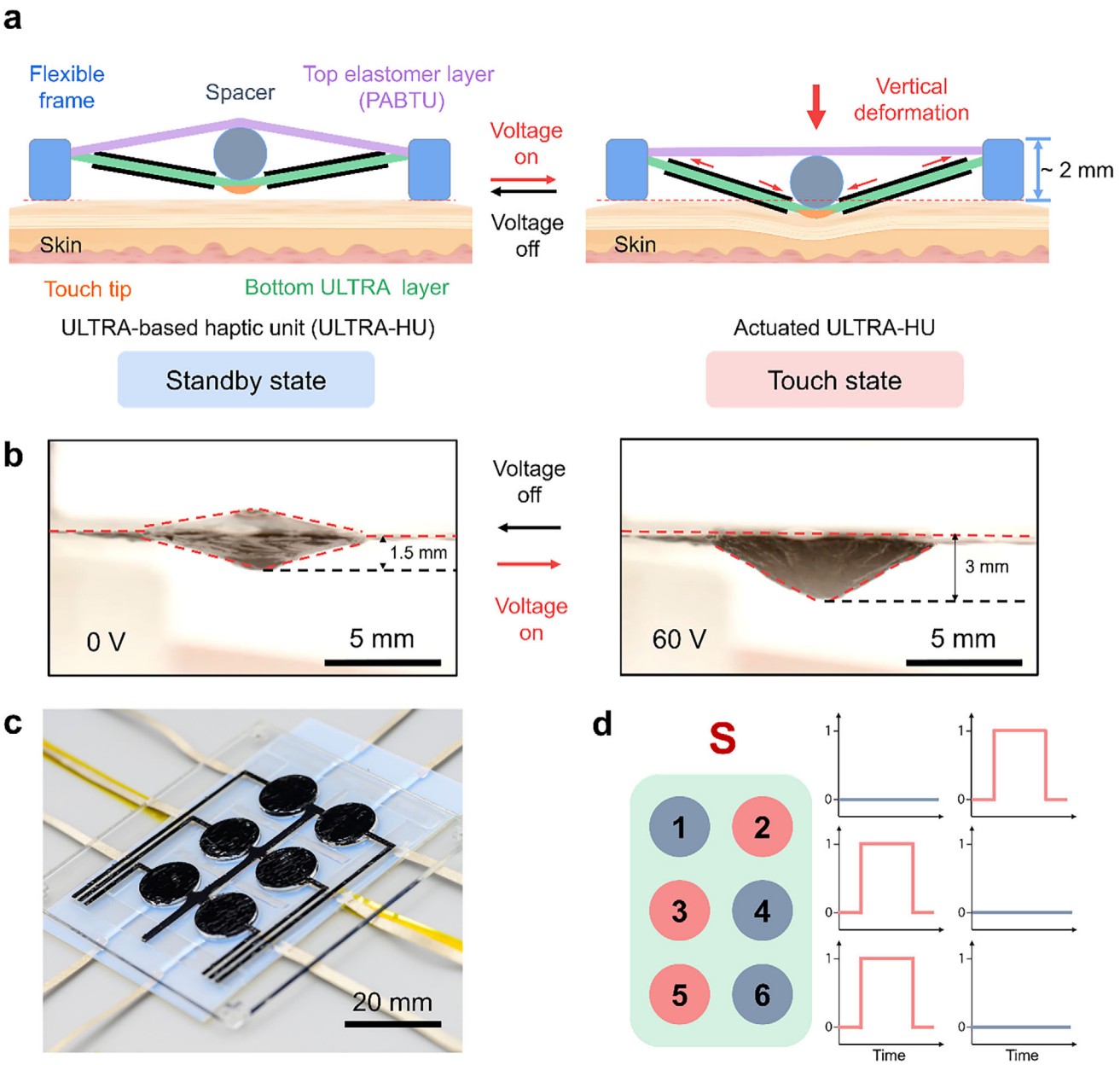

FIGURE 4 | ULTRA-based multipixel DEA array. (a) Illustration of potential use of ULTRA-based haptic unit (ULTRA-HU) in the standby state (left) and touch state (right). (b) Photographs of the prepared ULTRA-HU in the standby state (left) and touch state (right, 60 V). Red dash line shows the edge of ULTRA-HU. (c) Photo of the prepared multipixel array of ULTRA. (d) Example of the specific information that can be delivered by the Braille-like ULTRA array. It shows the specific letter S by controlling the input signal of each pixel.

were designed to have similar mechanical properties (modulus, thickness, and stretchability), so that in the standby state (voltage off), the elastic force of top elastomer layer was equal to that of bottom actuator layer, and thus there was a gap between the touch tip and skin. In the touch state (voltage on), the actuation further pushes the layer downwards and makes the tip touch the skin with force (Figure 4a). The signal delivered to the skin can be controlled by changing the driving frequency and voltage, and the pressure magnitude can also be adjusted by changing the tip diameter.

Based on the above ULTRA, as a proof of concept, we show two DEA designs using our high-k elastomer for potential haptic interfaces with a single ULTRA-HU under different frequencies and voltages (Figure 4b) and multipixel ULTRA array (Figure 4c). From 0.1to 10 Hz, ULTRA-HU showed rapid repeated response and recovery (Video S10). Furthermore, each pixel from multipixel ULTRA performed vertical deformation, and Figure 4d illustrates the standby state of actuator as blue and actuated state as red to mimic Braille-like communication. However, it should be noted that the array is ~10 times larger than the standard Braille size and the demonstration only shows the possibility of multipixel DEAs. The corresponding signals for each of the six pixels are represented as '0' for the standby state (voltage off) and '1' for the actuated state (voltage on). To write 'S' in Braille, pixels 1, 4, and 6 remained in the standby state, while pixels 2, 3, and

15214095, 0, Downloaded from https://advanced.onlinelibrary.wiley.com/doi/10.1002/adma.202523659 by Peking University Health, Wiley Online Library on [30/08/2026]. See the Terms and Conditions (https://onlinelibrary.wiley.com/terms-and-conditions) on Wiley Online Library for rules of use; OA articles are governed by the applicable Creative Commons License

5 were actuated to the touch state. Video S11 demonstrated the use of Braille-like ULTRA to convey specific information (such as STANFORD).

3 | Conclusion

We developed a skin-inspired molecular design strategy for low voltage DEAs using high-κ self-healing poly-(acrylonitrile-co-butadiene)-co-thiourea (PABTU). PABTU addresses three requirements that are challenging to be achieved simultaneously in a dielectric elastomer: a high dielectric constant (15 at 1 kHz), a low Young's modulus (0.58 MPa, and 0.012 MPa upon prestretch), and the ability to form ultrathin films (~ 3 μm) suitable for low voltage actuation. However, single layer PABTU showed relatively high dielectric loss, which leads to heating and lower breakdown strength (~33 V/μm). To mitigate this trade off, we implemented a PABTU/PDMS-$MPU_{0.3}$-$IU_{0.7}$ bilayer structure (ULTRA), increasing breakdown strength (~43 V/μm). Leveraging these combined properties, ULTRA DEAs show visible actuation at 30 V and achieve > 130% areal strain at 120 V, representing an approximately order of magnitude reduction in driving voltage compared with previously reported DEAs at comparable areal strains. We also demonstrated a low voltage multipixel actuator array and ULTRA-HU, highlighting its potential for low voltage wearable actuator concept. Despite achieving large areal strain at <100 V as a thin film DEA, additional works such as increasing Young's modulus or multistacking are needed to address output force for practical haptic and wearable implementations.

4 | Experimental Section

4.1 | Materials and Characterization

Carboxyl-terminated poly(acrylonitrile-co-butadiene) (CPAB, acrylonitrile content 26%, with a molecular weight M_n of 7800 g mol^{-1}, determined by GPC using narrow polydispersity polystyrene as standards and tetrahydrofuran (THF) as eluent at 40°C) was purchased from Scientific Polymer Products Inc. 1,3-dicyclohexylcarbodiimide (DCC), N-hydroxysuccinimide (NHS), ethanediamine, 1,4-butane diisothiocyanates, 1,4-diisocyanatobutane, carboxyl-terminated polybutadiene (CPB, with a molecular weight M_n of 7200 g mol^{-1} by GPC), Nitrile rubber (NBR, acrynitrile 37–39 wt.%), anhydrous dichloromethane (DCM), methanol (MeOH) were purchased from Sigma-Aldrich and used as received. Poly(vinylidene fluoride-co-hexafluoropropene) (P(VDF-HFP), 3M Dyneon) was used as received. ^{1}H NMR spectra (500 MHz) were recorded on a Bruker DRX 500 NMR spectrometer in deuterated solvents at 25°C. The chemical shift data for each signal are reported in units of δ (ppm). Fourier transform infrared spectra (FT-IR) were recorded on a Bruker Tensor 27 FT-IR spectrophotometer by 32 scans from 4000 to 600 cm^{-1}, with a resolution of 4 cm^{-1}. GPC was measured with a Tosoh Room-temperature Gel Permeation Chromatography EcoSEC by using THF as the solvent at 40°C. Differential Scanning Calorimetry (DSC) curves were measured with a TA Q2000 under a dry nitrogen atmosphere (50 mL min^{-1}). The experimental temperature is between −70°C and 120°C with a ramp rate of 10°C min^{-1} under a nitrogen atmosphere. The measurements of each sample were performed with two cycles and the curves of the second cycle were used. Uniaxial tensile measurements were performed on an Instron 5565 equipped with a 100 N load cell with a specific strain rate at 25°C. The photographs and videos were taken by mirrorless cameras. UV–vis-NIR spectra were collected on an Agilent Cary 6000i model. Film thickness values were measured using a contact probe Dektak 150 profilometer. Small-angle -ray scattering (SAXS) was conducted in transmission mode on bulk polymer films at a beamline 4-2 at Stanford Synchrotron Radiation Lightsource (SSRL) of SLAC National Accelerator Laboratory (SLAC, Menlo Park, CA). Bulk polymer films were tested as free-standing films with a thickness of 0.05 mm on the polyimide film frame. The x-ray wavelength was 0.827 Å (beam energy 15 keV) with a sample-to-detector distance of 3.512 m. IgorPro (Wavemetrics Inc.) was used for plotting and processing the SAXS data.

4.2 | Synthesis of Poly(Acrylonitrile-Co-butadiene)-Co-Thiourea (PABTU)

CPAB (10 g, ~1.4 mmol), and DCC (2.88 g, 14 mmol) were charged into a 100 mL flask and dissolved in 50 mL of anhydrous DCM. The reaction solution was stirred under an ice bath (0°C) in N_2 for 1 h, and then added NHS (1.6 g, 14 mmol) into the reaction and stir for 48 h. As the reaction progresses, the solution gradually becomes turbid and precipitates are formed. After the reaction, the solution was filtered and the filtrate was collected. The filtrate was dropwise added into the ethanediamine solution (8.4 g, 140 mmol, in 30 mL anhydrous DCM) with stirring under an ice bath in N_2. The reaction was continued with the protection of nitrogen at room temperature for 72 h. The solution was concentrated to a total volume of 50 mL and then precipitated in 300 mL methanol to give a viscous liquid polymer. It was re-dissolved in DCM (50 mL) and reprecipitated in methanol (300 mL), repeated two times to remove impurities. The viscous liquid polymer was dried under house vacuum at 70°C for 12 h and APAB was obtained as a light-yellow viscous liquid (7.9 g, 77% yield, Figure S1a). PABTU was prepared by the polymerization reaction between APAB and 1,4-butane diisothiocyanates (Figure S1c). The typical procedures for the preparation of PABTU is as follows: APAB (1 g, 0.14 mmol) was dissolved in 10 mL anhydrous DCM and stirred for 1 h, then a solution of S in DCM (0.025 g, 0.14 mmol) was added dropwise under room temperature. The resulting mixture was stirred for 24 h at RT under N_2. After the reaction, the solution was concentrated to about 3 and 15 mL MeOH was poured into it. The white precipitate-like viscous liquid appeared and the mixture was settled for 30 min at RT and then precipitate was collected. 10 mL DCM was added to dissolve the precipitate and then the concentration–precipitation process was repeated three times. The final polymer was collected by removing the solvent of DCM and MeOH under a vacuum.

4.3 | Mechanical Characterizations

Rectangular samples (~10 × 5 × 0.5 mm) were prepared. Room-temperature tensile test was performed at a crosshead speed of 50 mm/min. Stress relaxations tests were conducted by stretching the samples to a designated strain and then holding the strain constant while recording the force as a function of time. Cyclic

15214095, 0, Downloaded from https://advanced.onlinelibrary.wiley.com/doi/10.1002/adma.202523659 by Peking University Health, Wiley Online Library on [30/08/2026]. See the Terms and Conditions (https://onlinelibrary.wiley.com/terms-and-conditions) on Wiley Online Library for rules of use; OA articles are governed by the applicable Creative Commons License

stretching tests were performed by first pre-stretching the PABTU samples to 400% strain, followed by cyclic loading (50%, 100%, and 150% strain) for 100 cycles.

4.4 | Self-Healing Properties Characterization

To demonstrate self-healing properties of PABTU with cut and punctures, PABTU films (~30 × 5 × 0.5 mm) were either cut with a scalpel or punctured using a sharp needle (diameter: ~ 0.1 mm). PABTU film (~ 80 × 4 × 4 mm) was cut into four pieces of ~20 × 4 × 4 mm. The damaged films were gently pressed together to ensure the contact at the cut interfaces. To show the notch-insensitivity, PABTU film (~5 × 4 × 0.5 mm) was notched (notch length ~ 2 mm) and then stretched to > 2000% strain at cross speed of 50 mm/min.

4.5 | Dielectric Characterizations

The characterizations of the capacitance and phase angle of impedance were measured with a biologic VMP3 system by impedance spectroscopy over a frequency range from 100 mHz to 10 kHz. The corresponding dielectric constant of the polymer was calculated by the equation of $\varepsilon = (C \cdot t)/ (\varepsilon_0 \cdot A)$, where C is the measured capacitance, ε_0 is the permittivity of free space (8.85 $\times 10^{-12}$ F m^{-1}), t is the thickness of polymer film and A is the area of the counter electrode. The thickness of the dielectric layer was measured with a contact profilometer. The typical dimensions used for this measurement are with the thickness of about 500 nm and diameter of the counter electrode 4 mm. The polymer film was baked for 2 h at 150°C.

4.6 | ULTRA Fabrication and Actuation Properties

The as-prepared PABTU-based bilayer polymer film was fixed on a poly(methyl methacrylate) (PMMA) based stretchable frame with the initial diameter of 20 mm, then the polymer film was equixially stretched to four times its original diameter (Figure S24a). Then the compliant electrode with a 15 mm diameter was fabricated by coating carbon grease (MG Chemicals - 846) onto both sides of films and obtain the ULTRA. For the ULTRA with vertical deformation, a circular ring with an inner diameter of 15 mm was added to one side of the PABTU-based bilayer polymer film and then painted the electrode. The applied voltage was increased from 0 V to a maximum voltage of 120 V with the frequency range of 0.1to 200 Hz. The mirrorless camera was used to record the actuation behavior. The actuated area strain and actuated displacement were calculated by analyzing the related frame of the recorded videos. The actuation strain was calculated by the following equation:

$$\text{Areal strain } (\%) = \left(\frac{A_{max} - A_0}{A_0} \right) \times 100$$

where $A_{\max}$ is the maximum electrode area actuated at 0.5 Hz and A_0 is the initial electrode area without actuation. The initial circular car bon grease electrode diameter was 15 mm. For each measurement, at least three samples were tested.

Author Contributions

J.-C.L., and Z.B. conceived the idea. J.-C.L. synthesized PABTU. J.-C.L. and E.K. characterized material properties. J.-C.L., E.K., and C.X. fabricated dielectric elastomer actuators. S.N. designed the flexible printed circuit board for wireless wearable interface. All authors contributed to the discussion and interpretation of the results. J.-C.L., E.K., and Z.B. cowrote and revised the manuscript. Z.B. directed the project. J.-C.L., E.K., C.X., and S.N. contributed equally to this work.

Acknowledgements

Z.B. is a Chan Zuckerberg Biohub San Francisco investigator and an Arc Institute innovation investigator. Z.B. acknowledges support from the Tianqiao and Chrissy Chen Ideation and Prototyping Lab and Stanford Wearable Electronics Initiative (eWEAR) seed funding. The authors thank Yi Man Liu and Sai Fu Feng for their generous support of the Bao Group's research at Stanford University. E.K. acknowledges support from the Stanford Graduate Fellowship. C.Z. acknowledges funding from an F32 fellowship from the National Institute of Biomedical Imaging and Bioengineering of the National Institutes of Health (F32EB034156). Part of this work was performed at the Stanford Nano Shared Facilities (SNSF) RRID:SCR_023230, supported by the National Science Foundation under award ECCS-2026822.

Conflicts of Interest

The authors declare no conflicts of interest.

Data Availability Statement

The data that support the findings of this study are available from the corresponding author upon reasonable request.

References

1. P. Brochu and Q. Pei, "Advances in Dielectric Elastomers for Actuators and Artificial Muscles," *Macromolecular Rapid Communications* 31 (2010): 10–36.

2. M. Duduta, E. Hajiesmaili, H. Zhao, R. J. Wood, and D. R. Clarke, "Realizing the Potential of Dielectric Elastomer Artificial Muscles," *Proceedings of the National Academy of Sciences* 116 (2019): 2476–2481.

3. S. Jung, M. Kang, and M.-W. Han, "Dielectric Elastomer Actuators With Enhanced Durability by Introducing a Reservoir Layer," *Polymers* 16 (2024): 1277.

4. F. Carpi, S. Bauer, and D. De Rossi, "Stretching Dielectric Elastomer Performance," *Science* 330 (2010): 1759–1761.

5. G. Li, X. Chen, F. Zhou, et al., "Self-powered Soft Robot in the Mariana Trench," *Nature* 591 (2021): 66–71.

6. C. Xu, G. T. Stiubianu, and A. A. Gorodetsky, "Adaptive Infrared-Reflecting Systems Inspired by Cephalopods," *Science* 359 (2018): 1495–1500.

7. C. H. Li, C. Wang, C. Keplinger, et al., "A Highly Stretchable Autonomous Self-healing Elastomer," *Nature Chemistry* 8 (2016): 618–624.

8. H. Deyhle, S. Mushkolaj, and M. Wieland, "The Challenges in Artificial Muscle Research to Treat Incontinence," *Swiss Medical Weekly* 139 (2009): 591.

9. Z. Suo, "Theory of Dielectric Elastomers," *Acta Mechanica Solida Sinica* 23 (2010): 549–578.

10. R. Pelrine, R. Kornbluh, Q. Pei, and J. Joseph, "High-Speed Electrically Actuated Elastomers With Strain Greater than 100%," *Science* 287 (2000): 836–839.

11. G. Kofod, "The Static Actuation of Dielectric Elastomer Actuators: How Does Pre-stretch Improve Actuation?," *Journal of Physics D: Applied Physics* 41 (2008): 215405.

15214095, 0, Downloaded from https://advanced.onlinelibrary.wiley.com/doi/10.1002/adma.202523659 by Peking University Health, Wiley Online Library on [30/08/2026]. See the Terms and Conditions (https://onlinelibrary.wiley.com/terms-and-conditions) on Wiley Online Library for rules of use; OA articles are governed by the applicable Creative Commons License

12. E. Hajiesmaili and D. R. Clarke, "Dielectric Elastomer Actuators," *Journal of Applied Physics* 129 (2021): 151102.

13. D. M. Opris, "Polar Elastomers as Novel Materials for Electromechanical Actuator Applications," *Advanced Materials* 30 (2018): 1703678.

14. A. Poulin, S. Rosset, and H. R. Shea, "Printing Low-voltage Dielectric Elastomer Actuators," *Applied Physics Letters* 107 (2015): 244104.

15. M. W. M. Tan, G. Thangavel, and P. S. Lee, "Rugged Soft Robots Using Tough, Stretchable, and Self-Healable Adhesive Elastomers," *Advanced Functional Materials* 31 (2021): 2103097.

16. J. von Szczepanski and D. M. Opris, "High-Permittivity Polysiloxanes for Solvent-Free Fabrication of Dielectric Elastomer Actuators," *Advanced Materials Technologies* 8 (2023): 2201372.

17. Y. Sheima, P. Caspari, and D. M. Opris, "Artificial Muscles: Dielectric Elastomers Responsive to Low Voltages," *Macromolecular Rapid Communications* 40 (2019): 1900205.

18. L. J. Yin, Y. Zhao, J. Zhu, et al., "Soft, Tough, and Fast Polyacrylate Dielectric Elastomer for Non-magnetic Motor," *Nature Communications* 12 (2021): 4517, https://doi.org/10.1038/s41467-021-24851-w.

19. Y. Shi, E. Askounis, R. Plamthottam, et al., "A Processable, High-performance Dielectric Elastomer and Multilayering Process," *Science* 377 (2022): 228–232.

20. Z. Chen, Y. Xiao, J. Fang, et al., "Ultrasoft-yet-strong Pentablock Copolymer as Dielectric Elastomer Highly Responsive to Low Voltages," *Chemical Engineering Journal* 405 (2021): 126634.

21. Z. Ma, Y. Xie, J. Mao, X. Yang, T. Li, and Y. Luo, "Thermoplastic Dielectric Elastomer of Triblock Copolymer With High Electromechanical Performance," *Macromolecular Rapid Communications* 38 (2017): 1700268.

22. W. Feng, L. Sun, Z. Jin, et al., "A Large-strain and Ultrahigh Energy Density Dielectric Elastomer for Fast Moving Soft Robot," *Nature Communications* 15 (2024): 4222.

23. C. Stefaniu, P. L. Zaffalon, A. Carmine, et al., "Rigid Urea and Self-Healing Thiourea Ethanolamine Monolayers," *Langmuir* 31 (2015): 1296–1302.

24. Y. Yanagisawa, Y. Nan, K. Okuro, and T. Aida, "Mechanically Robust, Readily Repairable Polymers via Tailored Noncovalent Cross-linking," *Science* 359 (2018): 72–76.

25. J. Kang, D. Son, G. J. N. Wang, et al., "Tough and Water-Insensitive Self-Healing Elastomer for Robust Electronic Skin," *Advanced Materials* 30 (2018): 1706846.

26. C. B. Cooper and Z. Bao, "Using Periodic Dynamic Polymers to Form Supramolecular Nanostructures," *Accounts of Materials Research* 3 (2022): 948–959.

27. M. Herail, M. Berthelot, and A. Proutiere, "Prediction of Hydrogen Bond Basicity in Nitriles From Dipole Moments, Mesomeric Effects and Electrostatic Potentials," *Journal of Physical Organic Chemistry* 8 (1995): 421–428.

28. L. Chen, Z. Jin, W. Feng, L. Sun, H. Xu, and C. Wang, "A Hyperelastic Hydrogel With an Ultralarge Reversible Biaxial Strain," *Science* 383 (2024): 1455–1461.

29. J. Chen, Z. Pei, B. Chai, et al., "Engineering the Dielectric Constants of Polymers: From Molecular to Mesoscopic Scales," *Advanced Materials* 36 (2024): 2308670.

30. P. B. Ishai, M. S. Talary, A. Caduff, E. Levy, and Y. Feldman, "Electrode Polarization in Dielectric Measurements: A Review," *Measurement Science and Technology* 24 (2013): 102001.

31. T. Vu-Cong, C. Jean-Mistral, and A. Sylvestre, "Impact of the Nature of the Compliant Electrodes on the Dielectric Constant of Acrylic and Silicone Electroactive Polymers," *Smart Materials and Structures* 21 (2012): 105036.

32. G. Kofod, P. Sommer-Larsen, R. Kornbluh, and R. Pelrine, "Actuation Response of Polyacrylate Dielectric Elastomers," *Journal of Intelligent Material Systems and Structures* 14 (2003): 787–793.

33. J. Kang, J. Mun, Y. Zheng, et al., "Tough-Interface-Enabled Stretchable Electronics Using Non-Stretchable Polymer Semiconductors and Conductors," *Nature Nanotechnology* 17 (2022): 1265–1271.

34. L. Yang, M. Hao, K. Yang, et al., "A Review of Methods and Applications for Improving Electric Driving Performance of Dielectric Elastomer," *IEEE Transactions on Dielectrics and Electrical Insulation* 32 (2025): 117–126.

35. D. Yang, M. Tian, D. Li, W. Wang, F. Ge, and L. Zhang, "Enhanced Dielectric Properties and Actuated Strain of Elastomer Composites With Dopamine-Induced Surface Functionalization," *Journal of Materials Chemistry A* 1 (2013): 12276.

36. C. Zhang, W. Wei, H. Sun, and Q. Zhu, "Study on the Properties of Different Dielectric Elastomers Applying to Actuators," *Sensors and Actuators A: Physical* 329 (2021): 112806.

37. J. Huang, X. Zhang, R. Liu, Y. Ding, and D. Guo, "Polyvinyl Chloride-based Dielectric Elastomer With High Permittivity and Low Viscoelasticity for Actuation and Sensing," *Nature Communications* 14 (2023): 1483.

38. X. Ji, X. Liu, V. Cacucciolo, et al., "Untethered Feel-Through Haptics Using 18-μm Thick Dielectric Elastomer Actuators," *Advanced Functional Materials* 31 (2021): 2006639.

39. E. Kim, J.-C. Lai, L. Michalek, et al., "A Transparent, Patternable, and Stretchable Conducting Polymer Solid Electrode for Dielectric Elastomer Actuators," *Advanced Functional Materials* 35 (2025): 2411880.

40. C. Tang, B. Du, S. Jiang, Z. Wang, X.-J. Liu, and H. Zhao, "A Review on High-Frequency Dielectric Elastomer Actuators: Materials, Dynamics, and Applications," *Advanced Intelligent Systems* 6 (2024): 2300047.

Supporting Information

Additional supporting information can be found online in the Supporting Information section.

Supporting File 1: adma74559-sup-0001-SuppMat.pdf
Supporting File 2: adma74559-sup-0002-MovieS1.mp4
Supporting File 3: adma74559-sup-0003-MovieS2.mp4
Supporting File 4: adma74559-sup-0004-MovieS3.mp4
Supporting File 5: adma74559-sup-0005-MovieS4.mp4
Supporting File 6: adma74559-sup-0006-MovieS5.mp4
Supporting File 7: adma74559-sup-0007-MovieS6.mp4
Supporting File 8: adma74559-sup-0008-MovieS7.mp4
Supporting File 9: adma74559-sup-0009-MovieS8.mp4
Supporting File 10: adma74559-sup-0010-MovieS9.mp4
Supporting File 11: adma74559-sup-0011-MovieS10.mp4
Supporting File 12: adma74559-sup-0012-MovieS11.mp4

15214095, 0, Downloaded from https://advanced.onlinelibrary.wiley.com/doi/10.1002/adma.202523659 by Peking University Health, Wiley Online Library on [30/08/2026]. See the Terms and Conditions (https://onlinelibrary.wiley.com/terms-and-conditions) on Wiley Online Library for rules of use; OA articles are governed by the applicable Creative Commons License